Journal of Hydrology 588 (2020) 125013

Contents lists available at ScienceDirect

Journal of Hydrology

journal homepage: www.elsevier.com/locate/jhydrol

Research papers

Future hydropower generation prediction of large-scale reservoirs in the upper Yangtze River basin under climate change

Wenjie Zhong[a,b], Jing Guo[c], Lu Chen[a,b,*], Jianzhong Zhou[a,b], Junhong Zhang[d], Dangwei Wang[e]

[a] College of Hydropower & Information Engineering, Huazhong University of Science and Technology, Wuhan 430074, China
[b] Hubei Key Laboratory of Digital Valley Science and Technology, Wuhan 430074, China
[c] PowerChina Huadong Engineering Corporation Limited, Hangzhou 311122, China
[d] Dept. of Environmental Engineering, South-Central University for Nationalities, Wuhan 430074, China
[e] State Key Laboratory of Simulation and Regulation of River Basin Water Cycle, China Institute of Water Resources and Hydropower Research, Beijing 100038, China

ARTICLE INFO

This manuscript was handled by G. Syme, Editor-in-Chief

Keywords:
Hydropower generation prediction
Climate change
Large-scale reservoirs
VIC hydrological model
The upper Yangtze River Basin

ABSTRACT

Climate change, which impacts the spatial and temporal distribution of water resources, has a significant influence on the future hydropower generation. Studying the future evolution pattern of hydropower generation under climate change is of great significance for the medium- and long-term hydropower prediction. The objective of this paper is to predict the future hydropower generation of large-scale reservoir groups under climate change. The innovation of this paper is that the macro-scale distributed hydrological model combined with the optimal operation model of large-scale reservoirs was proposed for hydropower generation prediction. The established model considers the specific operation processes of large-scale reservoir groups, including 62 reservoirs in the case study. First, the Statistical Downscaling Model (SDSM) was built, and the evolution trend of future rainfall and temperature was predicted. Second, the macro-scale distributed Variable Infiltration Capacity (VIC) model was built to predict the future runoff. Finally, the optimal operation generation model of large-scale reservoir groups was established to predict the trends of hydropower generation under climate change. Results demonstrate that under RCP2.6 scenario, there is no significant increase or decrease trend of hydropower generation in the future. But under RCP4.5 and RCP8.5 scenarios, the hydropower generation shows a growing trend, and the increase trend under RCP8.5 scenario is more obvious than that under RCP4.5 scenario. Thus, the development of hydropower generation is sensitive to climate change. This study can provide a reference for the long-term prediction of hydropower generation capacity in the upper Yangtze River Basin.

1. Introduction

Hydropower generation plays an irreplaceable role in modern power system (Feng et al., 2017; Chen et al., 2016; Shi et al., 2019; Chen et al., 2020). In 2015, China's hydropower installed capacity exceeded 300, 000 MW (Li et al., 2018). Active development of hydropower is an important way to ensure China's energy supply and promote low-carbon emission reduction (Chen et al., 2013; Chang et al., 2010). However, climate change directly affects the meteorological factors such as temperature, rainfall, and evaporation, and indirectly affects other factors such as soil moisture content and runoff, etc., which results in the redistribution of water resources in time and space and the increase or decrease of the total water resources (Chen et al., 2010; Huntington, 2006; Shi and Wang, 2015). Further, climate change has a profound impact on the hydropower generation capacity of basins (Fan et al., 2018). Therefore, it is of great significance to predict runoff and hydropower generation under climate change. The existing methods for predicting the future runoff can be divided into statistical and data driven approaches and physically based approaches (Solomatine et al., 2007; Chen et al., 2014a; Nourani et al., 2014). The former methods mainly include classical regression analysis, back propagation neural network, nonlinear time series analysis and fuzzy mathematical mothed, etc., which forecasts future runoff by establishing the statistical relationship between weather and runoff data (Chen et al., 2018; Chu et al., 2016; Chen et al., 2014b). The physically based approaches are based on the hydrological model to simulate the relationship between rainfall and runoff and deduce the evolution trend of runoff through the future rainfall. Those methods have certain physical mechanisms, because they take into accounts the characteristics of atmospheric circulation, basin runoff generation and confluence, which are now praised by the academia (Nilawar and Waikar, 2019; Liu et al., 2015a; Chen et al., 2012).

* Corresponding author.
E-mail address: chl8505@126.com (L. Chen).

https://doi.org/10.1016/j.jhydrol.2020.125013
Received 24 March 2020; Received in revised form 23 April 2020; Accepted 24 April 2020
Available online 29 April 2020
0022-1694/

Experts and scholars have conducted a series of studies on the prediction of hydropower generation under climate change based on these runoff prediction results. Some scholars have carried out the prediction of hydropower generation under climate change based on empirical models such as simplified reservoir regulations and regression models (van Vliet et al., 2016; Zhou et al., 2015; Liu et al., 2016; Kao et al., 2015). For example, Liu et al. (2016) predicted the future runoff, and estimated developed hydropower potential (DHP) under climate change based on a kind of reservoir regulation rules. Kao et al. (2015) built a regression model between runoff and hydropower generation to predict the future hydropower generation. Although these studies have considered the impact of climate change, they did not consider the specific process of reservoir operation. In fact, the hydropower generation capacity is not only related to input factors such as hydrometeorology information, but also depends on the basic characteristics of hydropower stations (Madani et al., 2014). Considering the reservoir operation process, the hydropower generation process may be simulated more precisely (Qin et al., 2020). Some scholars have predicted the hydropower generation of single reservoir considering the specific reservoir operation process under climate change (Qin et al., 2020; Yang et al., 2015; Raje and Mujumdar, 2010). Raje and Mujumdar (2010) studied the response of reservoir hydropower generation under climate change for India's Hirakud reservoir. Yang et al. (2015) predicted the hydropower generation and water supply of Danjiangkou Reservoir under climate change by an adaptive multi-objective operation model. However, these studies only took into accounts the specific operation process of a single reservoir.

Since the hydropower prediction is a type of dynamic, time-delay and nonlinear modeling problem, especially with the rapid increase of the number of hydropower stations. When establishing the optimal operation model of large-scale reservoirs, there is a problem of the "cruse of dimensionality" (Zhou et al., 2018). Moreover, since the intelligent algorithm can't solve the local convergence problem, it is difficult to establish a mathematical model for predicting the large-scale reservoirs hydropower generation considering climate change and the characteristics of reservoirs (Liu et al., 2015b; Afshar, 2013; Moreno, 2009; Li et al., 2014a). In order to alleviate the influence of "cruse of dimensionality" and simplify the modeling process, the existing hydropower generation capacity prediction methods mainly focus on the improved DP algorithms, such as the discrete differential dynamic programming (DDDP) and the progressive optimality algorithm (POA) (Cheng et al., 2014; Howson and Sancho, 1975). The decomposition-coordination (DC) is also an effective approach for the optimal operation of large-scale reservoir groups, which can decompose a large system into many subsystems and reduce the difficulty of single system optimal operation (Cohen, 1978; Li et al., 2014b). However, the hydropower generation prediction considering climate change and the specific operation processes of large-scale reservoirs still needs to be further studied.

The objective of this paper is to propose a future hydropower generation prediction method for large-scale reservoirs considering climate change and specific reservoir operation processes. The innovation of this paper is summarized as follows. The runoff prediction based on macro-scale distributed hydrological model combined with the optimal operation model of large-scale reservoirs was proposed to predict the future hydropower generation under climate change. Second, the macro-scale distributed VIC hydrological model of the whole upper Yangtze River Basin with an area of one million square kilometers was first established. Third, the optimal operation model of large-scale reservoir groups including 62 reservoirs was built. The proposed method overcomes the limitation that the current generation prediction methods did not consider the specific operation process or only consider the operation processes of single reservoir.

The main framework of the study is as follows. First, the data of the General Circulation Models (GCMs) under different Representative Concentration Pathways (RCPs) emission scenarios was used in this paper, and the statistical downscaling model was employed for downscaling the data of GCMs and predicting the future evolution trend of rainfall and temperature. Second, the macro-scale distributed VIC hydrological model was established to simulate the response of future runoff to climate change. Third, the optimal operation model of large-scale reservoir groups in the upper Yangtze River Basin was established. And based on the simulated runoff data, the trends of future hydropower generation in the basin under RCP2.6, RCP4.5 and RCP8.5 emission scenarios were predicted.

2. Methodologies

2.1. Future rainfall and temperature prediction

General Circulation Models can provide reliable long-term future climate data according to atmospheric circulation mechanism. The fifth phase of Coupled Model Intercomparison Project(CMIP5) collected the results of nearly 60 climate models from 23 climate model groups worldwide (Klausmeyer and Shaw, 2009). In this paper, the second generation Canadian Earth System Model (CanESM2) developed by Canadian Centre for climate Modeling and Analysis was selected, and its future climate simulation results under three emission scenarios, namely RCP2.6, RCP4.5, and RCP8.5 were obtained. Studies show that the CanESM2 model can well simulate climate change in China (Zhang et al., 2016; Birkinshaw et al., 2017; Chen and Frauenfeld, 2014). Because the GCMs are large-scale models, it is necessary to be downscaled to characterize the atmospheric motion laws at small and medium scales. Downscaling methods can be divided into two categories, namely statistical downscaling and dynamical downscaling (Wood et al., 2004; Zorita and von Storch, 1999). Since the dynamical downscaling method is complex, the statistical downscaling method was widely used in hydrology, because of easier construction, less calculation work and more flexible form (Charles et al., 1999). The SDSM model was selected to downscale the CanESM2 model, in order to transform the large-scale atmospheric motion information into climate information of the study area in this paper.

2.1.1. The principle of the statistical downscaling model

The principle of SDSM model is establishment of the statistical relationship between GCM-derived predictor variables (such as atmospheric pressure, humidity and wind speed) and the weather variables of the study area (such as daily maximum temperature, daily minimum temperature and daily rainfall) based on multiple regression analysis method. Then, the GCM-derived predictor variables were taken as inputs of the SDSM model to generate future temperature and rainfall sequences of the study area.

The core of SDSM model is to establish the statistical relationship model between the predictor variable (S) and the weather variable (X), whose equation is given by

$$X = F(\mathbf{S}) \tag{1}$$

where F is the statistical relationship between the large-scale predictor variable set S and the local weather variable X. The performance of the SDSM model can be evaluated by the determination coefficient, which is given by

$$R^2 = \frac{\left[\sum_{i=1}^{T}(X_{obs,i} - \overline{X}_{obs})(X_{sim,i} - \overline{X}_{sim})\right]^2}{\sum_{i=1}^{T}(X_{obs,i} - \overline{X}_{obs})^2 \bullet \sum_{i=1}^{T}(X_{sim,i} - \overline{X}_{sim})^2} \tag{2}$$

where $X_{\mathrm{obs},i}$ and $X_{\mathrm{sim},i}$ are the observed and predicted values of output variable at time i; T is the length of the period; and $\bar{X}_{\mathrm{obs}}$ and $\bar{X}_{\mathrm{sim}}$ are the mean observed and predicted values of the output variable.

Table 1
26 predictor variables and their physical meanings.

Predictor variables	Physical meanings	Predictor variables	Physical meanings
mslp	Mean sea level pressure	p5zh	500hpa divergence
p1_f	Near surface geostrophic airflow velocity	p8_f	850hpa geostrophic airflow velocity
p1_u	Near surface zonal velocity component	p8_u	850hpa zonal velocity component
p1_v	Near surface meridional velocity component	p8_v	850hpa meridional velocity component
p1_z	Near surface vorticity	p8_z	850hpa vorticity
p1th	Near surface wind direction	p850	850hpa geopotential height
p1zh	Near surface divergence	p8th	850hpa wind direction
p5_f	500hpa geostrophic airflow velocity	p8zh	850hpa divergence
p5_u	500hpa zonal velocity component	prcp	precipitation
p5_v	500hpa meridional velocity component	s500	500hpa relative humidity
p5_z	500hpa vorticity	s850	850hpa relative humidity
p500	500 hPa geopotential height	shum	Near surface specific humidity
p5th	500hpa wind direction	temp	Near surface air temperature

2.1.2. Screening of predictor variables of SDSM model

The screening of predictor variables is very important for the successful construction of SDSM model. Selecting the predictor variables with higher correlations with weather variables can help improve the accuracy of simulation. Daily maximum temperature, daily minimum temperature and daily rainfall were chosen as the weather variables. Table 1 gives the predictor variables to be screened and their physical meanings.

Historical data of 26 predictor variables from the National Centers for Environmental Prediction (NCEP) and historical weather variables data of the study area can be used as inputs to the SDSM model. The “Screen Variables” module of the SDSM model was employed to screen appropriate predictor variables. Based on this module, the statistical relationship between predictor variables and weather variables can be established. Then, users can select the appropriate predictor variables based on the correlation analysis between each predictor variable and weather variable, and the correlation measuring methods mainly include partial correlation analysis, seasonal correlation analysis and scatterplots.

And there are several optimization principles need to be noted in the process of selection. First, the predictor variables should be able to reflect the physical mechanism of the change of weather variables. Second, the results of correlation analysis between them should be good. Third, the selected predictors should be independent or weakly correlated. Last, the predictor variables should be common to GCMs data and NCEP data (Wilby et al., 1998).

2.1.3. Future weather variables prediction

During this section, the future daily rainfall and daily temperature were simulated according to the established multiple linear regression model between predictor variables and weather variables. For the simulation of daily rainfall, it can be divided into two parts: the simulation of rainfall incidence, and the simulation of precipitation. The regression equation of rainfall probability is as follows (Wilby et al., 1999):

$$O_t = \alpha_0 + \sum_{i=1}^{n} \alpha_i s_i + \alpha_{t-1} O_{t-1} \tag{3}$$

where O_{t-1} and O_t are rainfall probabilities at day t-1 and t; α_0 andα_i are parameters estimated using linear least squares regression; s_i is predictor variable i; α_{t-1} is the regression parameter of day t-1. Whether rainfall occurs is determined by a random number l_t between 0 and 1 that obeys the uniform distribution. If O_t is greater thanl_t, there will be rainfall in day t.

For the value of precipitation, the equation is given by (Wilby et al., 1999)

$$U_t = f_{\exp}\left[\phi\left(\beta_0 + \sum_{i=1}^{n} \beta_i s_i + \varepsilon\right)\right] \tag{4}$$

where U_t is the precipitation value of day t; $f_{\exp}$ is the empirical distribution function of precipitation value at day t; ϕ is the normal cumulative distribution function; β_0 andβ_i are parameters estimated using linear least squares regression; ε is random or modelling error.

For the temperature simulation, it is not necessary to simulate the possibility of occurrence, but only to simulate the random change of temperature value, whose calculation is similar to precipitation (Srikanthan and McMahon, 2001). After the calibration of the SDSM model, the GCMs data under different RCPs emission scenarios in the future are used as the inputs to the “Scenario Generator” module of the SDSM model. The future weather variables data under different RCPs emission scenarios can be generated.

2.2. Rainfall-runoff simulation based on the VIC hydrological model

In this study, the VIC hydrological model was used to simulate the future runoff. This model is a macro-scale distributed hydrological model, which is generally applied to basins with an area of tens of thousands of square kilometers. The VIC model can simulate vegetation transpiration, soil evaporation, canopy evaporation, snow accumulation and ablation, soil freeze–thaw, etc. Thus, it comprehensively characterizes the transfer paths and processes of various water bodies. The main modules of the VIC model include evapotranspiration, runoff generation and runoff confluence. The model transfers the whole basin into many grids, calculates the runoff generation, and then converts the output data of each grid into the flow process of the outlet section of the basin through the ‘Confluence Module’. The input files of the VIC model include soil data, vegetation data, meteorological forcing data, flow direction data, basin characteristics data and global parameter files etc. Parameters of the VIC model which need to be calibrated are shown in Table 2. After model calibration, the future weather data predicted by the SDSM model was used as inputs to the VIC hydrological model to simulate the future runoff.

Table 2
Parameters of the VIC model which need to be calibrated.

Parameters	Meanings	Ranges of values
b	Variable infiltration curve parameter	(0,1)
D_s	Fraction of D_m where non-linear base flow begins	(0,1)
D_m	Maximum velocity of base flow	(0,30)
W_s	Fraction of maximum soil moisture where non-linear base flow occurs	(0,1)
d_1	Depth of the first layer of soil(m)	(0,0.5)
d_2	Depth of the second layer of soil(m)	(0,2)
d_3	Depth of the third layer of soil(m)	(0,4)

The univariate search technique was used to calibrate the parameters of VIC model, and the Nash-Sutcliffe efficiency (*NSE*) and the relative error (e_{all}) of the observed and simulated flow data were chosen to assess the performance of the model.

$$NSE = 1 - \frac{\sum_{t=1}^{T} (Q_{\mathrm{obs}}^t - Q_{\mathrm{sim}}^t)^2}{\sum_{t=1}^{T} (Q_{\mathrm{obs}}^t - \bar{Q}_{\mathrm{obs}})^2} \tag{5}$$

$$e_{\mathrm{all}} = \frac{\left| \sum_{t=1}^{T} Q_{\mathrm{obs}}^t - \sum_{t=1}^{T} Q_{\mathrm{sim}}^t \right|}{\sum_{t=1}^{T} Q_{\mathrm{obs}}^t} \tag{6}$$

where Q_{obs}^t is the observed streamflow data at time t; Q_{sim}^t is the simulated streamflow data at time t; and $\bar{Q}_{\mathrm{obs}}$ is the mean value of observed streamflow data.

In the process of parameter calibration, the sensitivity analysis method based on perturbation analysis was used to analyze the sensitivity of parameters (Choi and Choi, 1992). The formula is given as follows:

$$S_{\mathrm{sen}} = \frac{1}{n-1} \cdot \sum_{i=1}^{n-1} \frac{(R_i + R_{i+1})/\bar{R}_{i,i+1}}{(P_i + P_{i+1})/\bar{P}_{i,i+1}} \tag{7}$$

where S_{sen} is the sensitivity index; n is the number of tests for the selected parameter; R_i and P_i are the evaluation index and the parameter value in the i^{th} test respectively; $\bar{R}_{i,i+1}$ and $\bar{P}_{i,i+1}$ are the average value of the evaluation index and the parameter value in the i^{th} and $i+1$th tests respectively. The larger the sensitivity index value is, the more sensitive the parameter is. If the sensitivity index value is more than 1, it means that this parameter is a sensitive parameter.

2.3. Establishment of the optimal operation model of large-scale reservoirs

The objective of the optimal operation model is to maximize the annual hydropower generation of large-scale reservoirs. The future runoff data simulated by the VIC model under different carbon emission scenarios were used as the inputs to the optimal operation model of large-scale reservoirs. DP is a powerful method in solving operation problem, however it is not applicable in this problem because of the "curse of dimensionality". So the discrete differential dynamic programming (DDDP) combined with the large-scale system decomposed-coordinating (LSSDC) method proposed by Li et al. (2014) were employed to solve the optimal models in order to deal with the dimensionality problems. The detailed information of the model is given below.

(1) Objective function: maximization of the annual hydropower generation

$$\max E = \sum_{i=1}^{S} \sum_{j=1}^{T} N_{ij} \Delta t, \; N_{ij} = A_i H_{ij} Q_{ij}^N \tag{8}$$

where E is the annual hydropower generation of large-scale reservoirs; S is the total number of reservoirs; T is the total number of periods; N_{ij} is the hydropower production of reservoir i at time j; A_i is the hydropower production coefficient of reservoir i; Δt is the time step of each period; H_{ij} is the available net head of reservoir i at time j; and Q_{ij}^N is the water discharge for hydropower generation of reservoir i at time j.

(2) The function is subject to the following constraints, including water level limits, reservoir discharge limits, hydropower generation limits, and water balance equation, etc.

① Water level limits:

$$Z_{ij}^{\min} \leqslant Z_{ij} \leqslant Z_{ij}^{\max} \tag{9}$$

$$Z_{i0} = Z_i^I, \; Z_{iT} = Z_i^F \tag{10}$$

where Z_{ij} is the water level of reservoir i at time j; $Z_{ij}^{\max}$ and $Z_{ij}^{\min}$ are the upper and lower water level limit of reservoir i at time j; and Z_i^{I} and Z_i^{F} are the initial and final water levels of reservoir i during the operating period.

② Reservoir discharge limits:

$$Q_{ij}^{\min} \leqslant Q_{ij} \leqslant Q_{ij}^{\max} \tag{11}$$

where Q_{ij} is the water discharge of reservoir i at time j; $Q_{ij}^{\max}$ and $Q_{ij}^{\min}$ are the upper and lower water discharge limit of reservoir i at time j.

③ Hydropower generation limits:

$$N_{ij}^{\min} \leqslant N_{ij} \leqslant N_{ij}^{\max} \tag{12}$$

where $N_{ij}^{\max}$ and $N_{ij}^{\min}$ are the installed capacity and minimum hydropower output constraints of reservoir i at time j.

④ Available net head of reservoirs:

$$H_{ij} = (Z_{ij} + Z_{i,j+1})/2 - f_i^{QZ}(Q_{ij}) \tag{13}$$

where H_{ij} is the available net head of reservoir i at time j; Z_{ij} and $Z_{i,j+1}$ are the water levels of reservoir i at the beginning of time j and $j+1$, respectively; and f_i^{QZ} is the function of downstream water level and water discharge.

⑤Water balance equation:

$$V_{i,j+1} = V_{ij} + (I_{ij} - Q_{ij})\Delta t \tag{14}$$

where V_{ij} and $V_{i,j+1}$ are the storages volumes of reservoir i at the beginning of time j and $j+1$, respectively; and I_{ij} is the inflow of reservoir i at time j.

⑥ Hydraulic connections between upstream and downstream reservoirs:

$$I_{ij} = \sum_{k \in \Omega_i} Q_{kj} + B_{ij} \tag{15}$$

where Ω_i is the set of the all nearest reservoirs upstream of reservoir i; Q_{kj} is the water discharge of reservoir k at time j; and B_{ij} is the local inflow of reservoir i at time j.

⑦Nonnegative constraints: all variables in the model should be greater than or equal to 0.

After the establishment of the optimal large-scale reservoir operation model, the future runoff sequences predicted by the VIC model were used as the inputs of the operation model to calculate the hydropower generation of the large-scale reservoirs.

3. Case study

The Yangtze River originated from the Geladandong peak of the Tanggula mountains. In the upper basin, its main tributaries include Yalong River, Minjiang River, Wujiang River and Jialing River. The upper Yangtze River Basin was selected as a case study, which located in the southwest of China. It is a big basin of one million square kilometers which accounts for about 10% of China's land area, and involves nine provinces, municipalities and autonomous regions. The topography of the basin is diverse, including plateau (the Qinghai-Tibet Plateau), basin (the Sichuan Basin), etc. Affected by the subtropical monsoon and the Qinghai-Tibet Plateau high-cold climate, rainfall and hydropower resources here are abundant, and meanwhile the climate here is very sensitive. Yichang station is the outlet of the upper Yangtze River Basin, and there are another six stations along the Yangtze River namely Shigu, Panzhihua, Xiluodu, Xiangjiaba, Zhutuo and Cuntan stations considered in this study, as shown in Fig. 1.

The historical NCEP re-analysis data of prediction variables (https://www.esrl.noaa.gov/), the historical rainfall and temperature data of the basin derived from the China Meteorological Data Center (http://data.cma.cn), and the future prediction variables data of

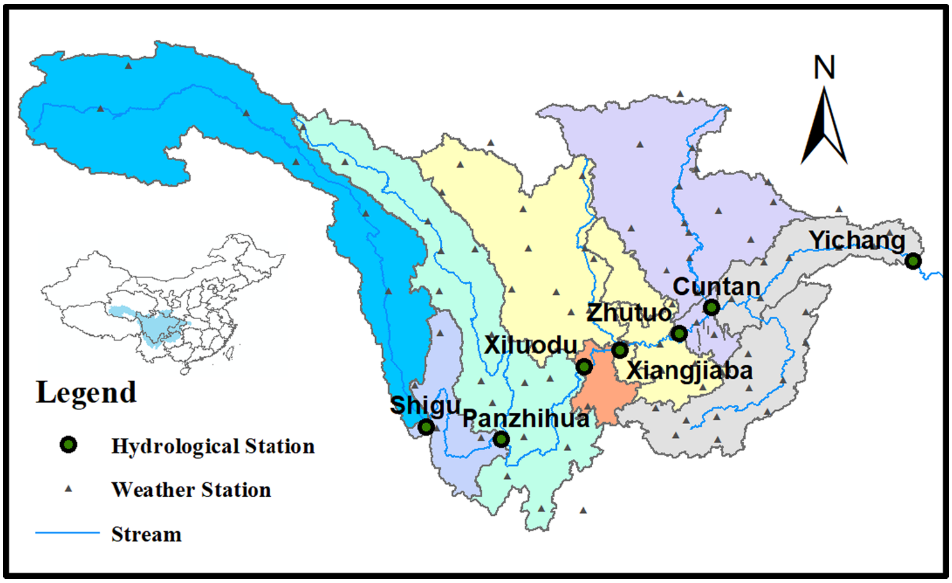

Fig. 1. The upper Yangtze River Basin and its corresponding gauging stations.

Fig. 2. Locations of reservoirs in the study area.

CanESM2 under three different emission scenarios downloaded from the Canadian Centre for Climate Modelling and Analysis (https://www.canada.ca/en.html), were used for the establishment of the SDSM model. The historical rainfall data, temperature data, runoff data of the basin and the DEM elevation data of 30 km spatial resolution from Geospatial Data (http://www.gscloud.cn), vegetation data from the University of Maryland (http://glcf.umd.edu/data/) and soil data from the Food and Agriculture Organization of the United Nations (http://www.fao.org/geonetwork) were used for the establishment of the VIC model. And the characteristic curves of 62 reservoirs in the upper Yangtze River Basin were collected to establish the optimal operation model of large-scale reservoirs. The study area and the scheme of the large reservoir system are given in Figs. 1 and 2.

4. Results and discussions

First, the SDSM model was established to predict the rainfall and temperature sequences under different emission scenarios; second, the VIC hydrological model was established to predict the future runoff; and third the optimal operation model of large-scale reservoirs was established to predict the future hydropower generation ability of the study area.

4.1. Future rainfall and temperature prediction

The NCEP re-analysis data (the predictor variables) and the historical rainfall and temperature data (the weather variables) were taken as inputs of SDSM model. The statistical relationship between the predictor variables and the weather variables were established based on SDSM model. The daily data from 1970 to 1999 were used for model

Table 3
Determination coefficients, fitted curves slopes and root mean square errors of each station.

Periods	Stations	Monthly rainfall			Monthly mean daily maximum temperature			Monthly mean daily minimum temperature		
		R^2	a	RMSE	R^2	a	RMSE	R^2	a	RMSE
Calibration period	Shigu	0.899	0.941	12.69	0.957	0.952	1.351	0.983	0.981	1.091
	Panzhihua	0.806	1.038	49.68	0.912	0.901	1.217	0.982	0.979	0.861
	Xiluodu	0.902	0.962	20.02	0.940	0.930	1.106	0.985	0.984	0.749
	Lizhuan	0.863	0.878	28.68	0.967	0.967	1.156	0.985	0.986	0.781
	Zhutuo	0.652	0.827	41.16	0.963	0.964	1.464	0.977	0.974	0.992
	Cuntan	0.764	0.784	33.03	0.969	0.967	1.403	0.976	0.969	1.018
	Yichang	0.710	0.803	36.75	0.964	0.964	1.481	0.979	0.977	0.976
	Whole basin	0.920	0.986	17.07	0.976	0.971	0.964	0.990	0.988	0.7131
Validation period	Shigu	0.933	0.909	10.56	0.962	1.013	1.289	0.987	1.001	1.128
	Panzhihua	0.870	1.090	42.09	0.927	0.978	1.021	0.983	1.004	0.912
	Xiluodu	0.929	0.917	16.68	0.951	1.003	1.005	0.986	1.001	0.821
	Lizhuan	0.877	0.932	24.99	0.976	0.984	0.996	0.989	0.995	0.716
	Zhutuo	0.578	0.835	46.52	0.970	0.974	1.301	0.983	1.004	0.927
	Cuntan	0.778	0.746	32.23	0.969	0.986	1.400	0.982	1.008	0.923
	Yichang	0.744	0.877	33.18	0.972	0.984	1.301	0.983	1.007	0.889
	Whole basin	0.929	0.991	15.45	0.981	1.008	0.878	0.993	1.008	0.697

calibration, and the daily data from 2000 to 2005 were used for model validation. Then the statistical relationships between the predictor variables and basin's rainfall and temperature data were determined. The determination coefficients (R^2), fitted curves slopes (a) and root mean square errors (RMSE) of the observed and simulated monthly data at each station in both calibration and validation periods were calculated, as shown in Table 3 and Figs. 3 to 4.

It can be seen from Figs. 3 and 4 and Table 3 that the simulation results of temperature at each station are excellent in both calibration and validation periods. Most of the determination coefficients are above 0.95, and the slopes of the curves are within the range of 0.901 to 1.013. And the RMSE values of daily maximum and minimum temperatures at each station are between 0.878 ~ 1.481℃ and 0.697 ~ 1.403℃ respectively. The simulation results of daily minimum temperature show a better performance than those of daily minimum temperature, for its determination coefficients are generally higher in both calibration and validation periods. Meanwhile, the RMSE values of daily minimum temperature at most stations are also lower than that those of daily maximum temperature in both calibration and validation periods. For rainfall simulation, the result is not as good as that of temperatures, since the rainfall simulation is more complex and discrete (Zhang et al., 2016; Hassan et al., 2014). The determination coefficients of rainfall at most stations reach 0.75 in both calibration and validation periods, except for Zhutuo station, and the slopes of the curves are within the range of 0.746 to 1.090. RMSE values of rainfall simulation at each station are acceptable, which are within 10% of the observed precipitation in both calibration and validation periods. For Zhutuo station, the rainfall simulation results are not so good, which may be affected by regional factors, such as topography.

For the whole basin, the performance of the SDSM model is also good. The determination coefficients of rainfall are all above 0.90, and the determination coefficients of maximum and minimum temperatures are generally above 0.95 in both calibration and validation periods. The RMSE values of the whole basin are also lower than those of most single stations. For rainfall simulation, the RMSE values are within 5% of the observed precipitation; and for temperature simulation, the RMSE values are less than 1.0℃. The variation range of monthly mean maximum and minimum temperatures were within ± 0.15℃, and the variation range of monthly rainfall is from −2mm to 11.4 mm in calibration period. In general, the simulation results of the SDSM model are perfect, and it and can be used for the future climate simulation of the study area.

Then, the future periods were divided into three stages, namely 2020 s (2018–2044), 2050 s (2045–2071) and 2080 s (2072–2100). The CanESM2 predictor variables data from 2018 to 2100 were taken as inputs of the SDSM model to predict the daily rainfall, daily maximum and minimum temperatures in the future period under different emission scenarios. The predicted annual weather variables of the whole basin are given in Fig. 5.

As shown in Fig. 5, the predicted weather variables data are fluctuated in different degrees. The rainfall data under RCP8.5 scenario shows a significant increasing trend, while the rainfall data under RCP2.6 scenario and RCP4.5 scenario shows a slight increasing trend. The trends of the temperature are similar to those of rainfall. Moreover, it is demonstrated that the main variation of rainfall during a year is basically concentrated in flood season. To the contrary, the variations of temperature is opposite, which change significantly in dry season. These results are similar to those of previous studies (Zhang et al., 2016). Taking the weather variables from 1970 to 2005 as baseline period, the trends of rainfall and temperature in each future period were analyzed, and results of the whole basin are given in Table 4.

As shown in Table 4, the maximum change rate of rainfall is19.90%, which occurred in 2080 s, and the maximum change rates of maximum and minimum daily temperatures are 8.24% and 18.74% respectively, both occurred in 2080 s. For RCP2.6 scenario, the trends of rainfall and the temperature increase first and then decrease, and the decrease of temperature is slightly larger. For RCP4.5 scenario, the rainfall and the temperature increase all the time. For RCP8.5 scenario, all the weather variables show an increasing trend, and their growth rates are much more rapid than those under RCP4.5 scenario, which agrees with the analysis of Tao et al. (2015).

4.2. Future runoff prediction

The VIC model was built to simulate the rainfall-runoff relationship. The DEM data was used to calculate the stream networks and obtain the sub-basin boundaries according to Shigu, Panzhihua, Xiluodu, Xiangjiaba, Zhutuo, Cuntan and Yichang stations. The basin area was transformed into grids of $0.5^{\circ} \times 0.5^{\circ}$ that can be distinguished by the VIC model, and the stream directions of each grid were calculated by the D8 algorithm. Then the vegetation and soil data, including the types and parameters of vegetation and soil, were extracted to each grid and the meteorological forcing data of weather stations were interpolated to each grid as well. Some of the input files are given in Figs. 6–8 and Tables 5 and 6.

The observed weather variables and runoff data from July 1, 2014 to June 30, 2017 was used for model calibration, and the data from July 1, 2017 to June 30, 2018 was used for model validation. In the calibration process, the sensitivity of each parameter was analyzed. The daily Nash efficiency coefficient NSE was selected as the evaluation index, and S_{sen} was the sensitivity index. Results of each station are shown in Table 7.

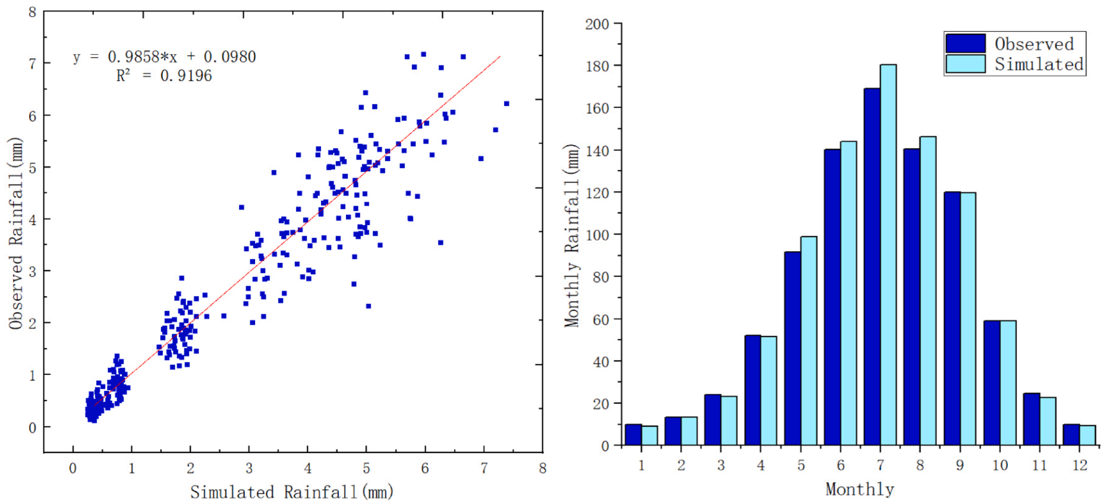

(a) Simulation results of daily rainfall

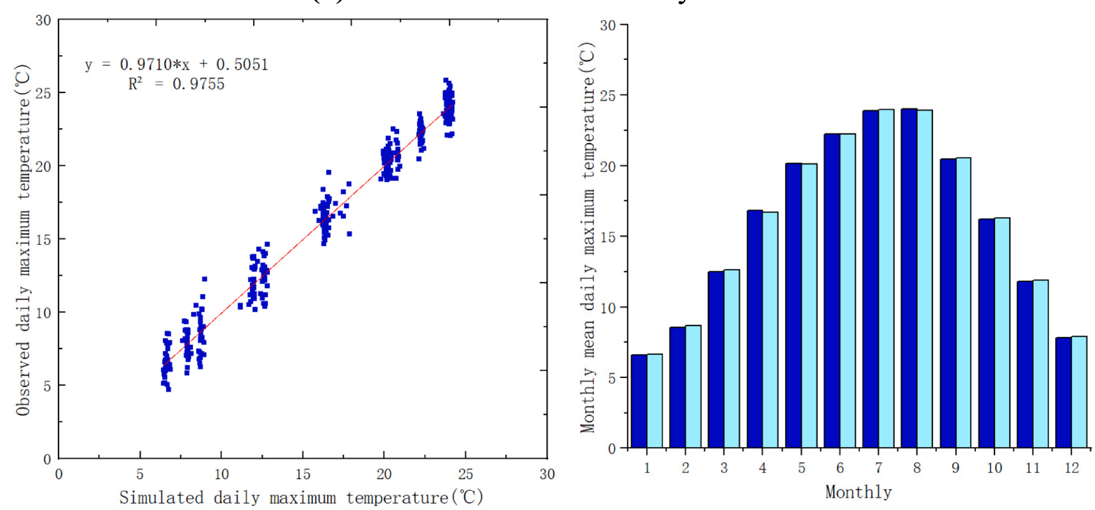

(b) Simulation results of daily maximum temperature

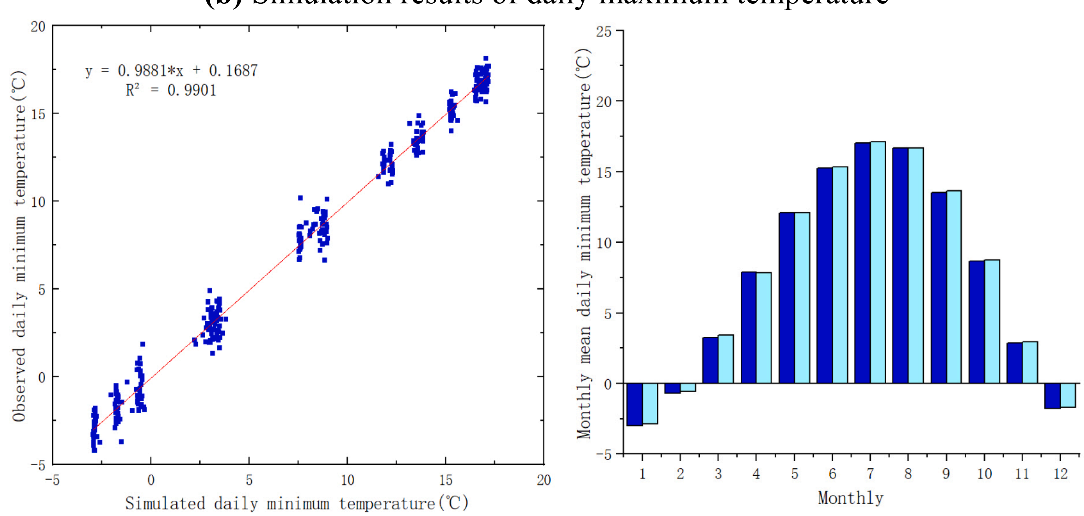

(c) Simulation results of daily minimum temperature

Fig. 3. Observed and simulated data of monthly weather variables in the calibration period.

It is indicated from Table 7 that the depth of the second layer of soil d_2 is the most sensitive parameter for each station, and it is the only parameter whose average sensitivity index exceeds 1. This is because the water storage capacity of the second layer of soil has a significant impact on the runoff generation. The greater the depth is, the stronger the water storage capacity is. Among the other parameters, the variable infiltration curve parameter *b* that can affect the rate of infiltration of water into the soil, is also a key parameter affecting the runoff

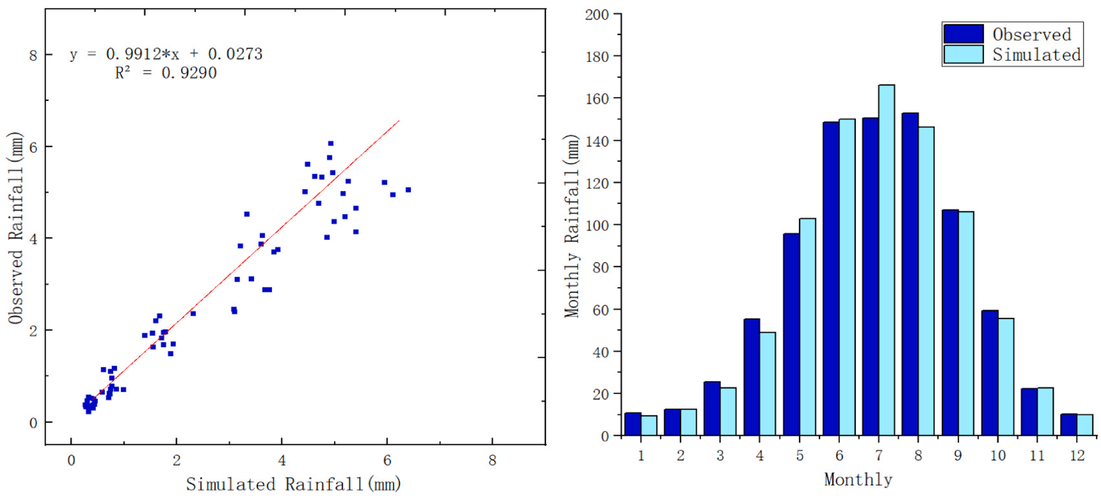

(a) Simulation results of daily rainfall

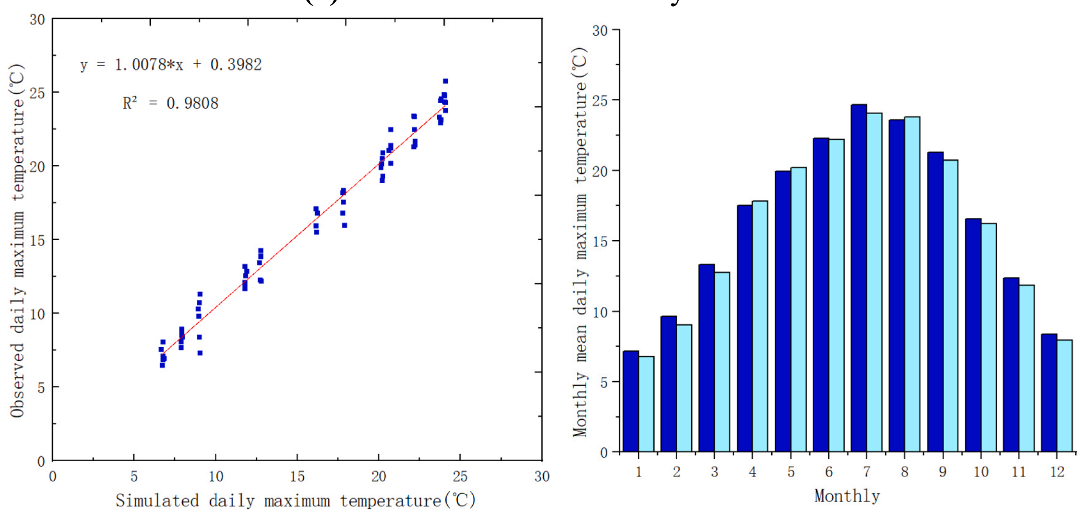

(b) Simulation results of daily maximum temperature

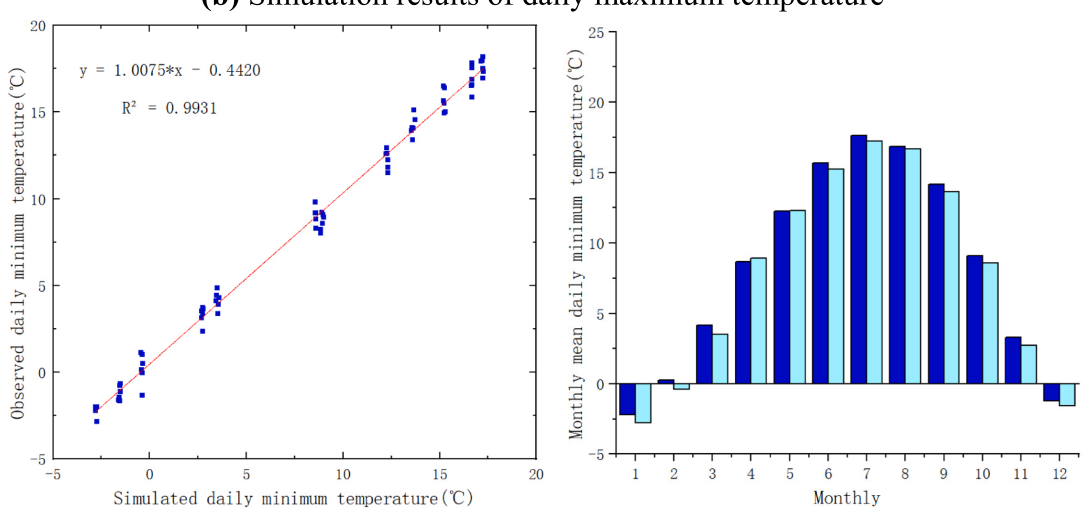

(c) Simulation results of daily minimum temperature

Fig. 4. Observed and simulated data of monthly weather variables in the validation period.

generation, whose sensitivity is also large. For the depth of the first layer of soil d_1, it can also affect the soil water storage. However, due to its small depth, its sensitivity is less than d_2. And among the soil depths, the depth of the third layer of soil d_3 is the least sensitive, because it mainly affects the base flow and the seasonal changes of soil water content. For the parameters D_s, D_m and W_s, they mainly affect the base flow. So they are less sensitive. These results are similar to the studies by Nijssen et al. (2001) and Su et al. (2005).

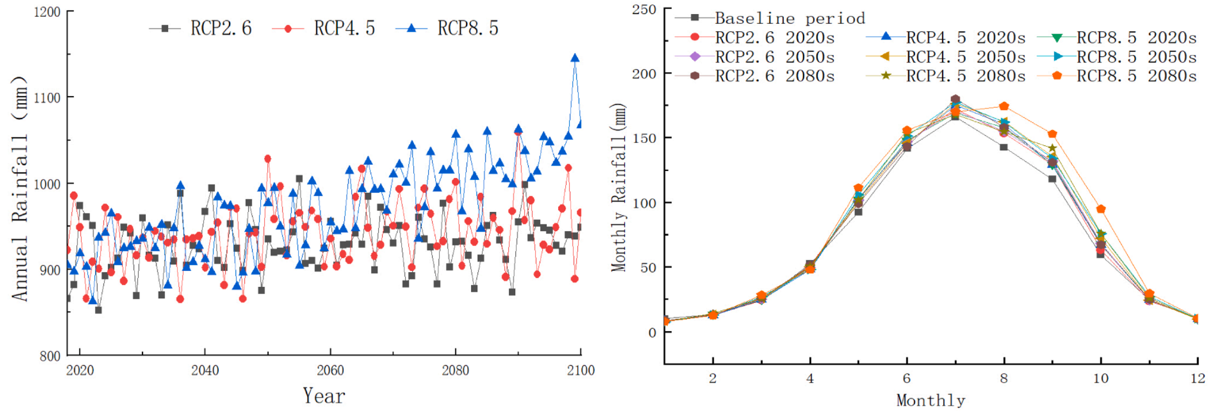

(a) Annual and monthly rainfall

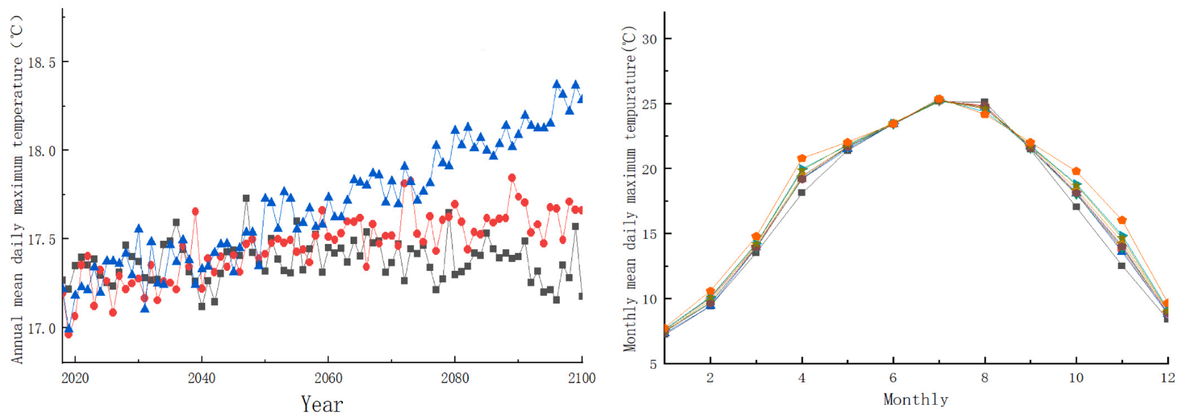

(b) Annual and monthly mean daily maximum temperature

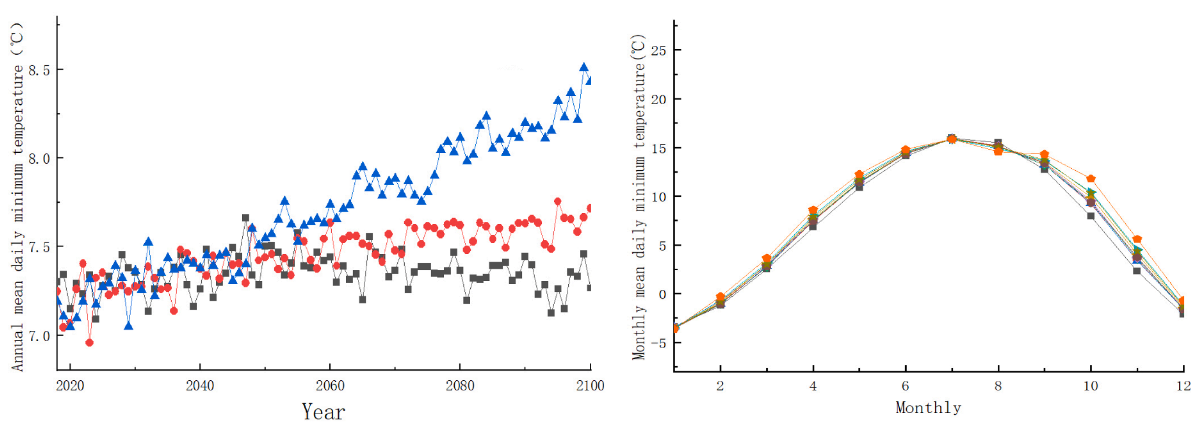

(c) Annual and monthly mean daily minimum temperature

Fig. 5. The predicted rainfall, daily maximum temperature and minimum temperature data from 2018 to 2100 under different RCPs scenarios.

The daily Nash efficiency coefficient NSE, monthly Nash efficiency coefficient NSE_{mon} and the relative error e_{all} of each station were chosen as the evaluation indexes of model calibration. Simulation results in calibration and validation periods are shown in Table 8.

According to Table 8, except for the Yichang station, the daily Nash efficiency coefficients are all above 0.80. In terms of monthly Nash efficiency coefficient, all of the stations are above 0.90 except for the Shigu station, and the Nash efficiency coefficients of some stations are more than 0.95. For the relative error between the observed and simulated flow, except for the Shigu station, the values of each station are generally below 0.05. Moreover, for the Yichang station, the simulated flood peak is slightly delayed compared with the observed value, which causes the error of daily runoff simulation. However, this error decreases and even can be ignored in monthly scale runoff prediction. This is maybe because that in daily runoff simulation, the errors accumulate in the process of runoff generation and concentration and reach a large value at the basin outlet. For the Shigu station, compared with the observed values, the simulated values are slightly smaller in the dry season and larger in the flood season. This error is not large in daily scale simulation, but the difference is amplified in monthly scale.

Table 4
Trends of rainfall and temperature data of the whole basin in the future periods.

Data types	Periods	Baseline period mean value	Predicted mean value			Change rate		
			RCP2.6	RCP4.5	RCP8.5	RCP2.6	RCP4.5	RCP8.5
Rainfall(mm/year)	2020 s	853.6	923.8	927.2	929.3	8.22%	8.62%	8.87%
	2050 s	853.6	932.6	947.8	963.1	9.25%	11.04%	12.83%
	2080 s	853.6	930.1	952.6	1023.5	8.96%	11.60%	19.90%
Maximum temperature(℃)	2020 s	16.90	17.33	17.27	17.33	2.54%	2.19%	2.54%
	2050 s	16.90	17.43	17.49	17.66	3.14%	3.49%	4.50%
	2080 s	16.90	17.36	17.62	18.06	2.72%	4.26%	6.86%
Minimum temperature(℃)	2020 s	6.83	7.30	7.29	7.31	6.88%	6.73%	7.03%
	2050 s	6.83	7.42	7.47	7.67	8.64%	9.37%	12.30%
	2080 s	6.83	7.33	7.60	8.11	7.32%	11.27%	18.74%

The monthly Nash efficiency coefficient values are smaller than other stations. In addition, the lack of meteorological stations in the upper reaches of Shigu station may be the cause of the simulation error. Generally, the VIC model has a good performance for the rainfall-runoff simulation for the upper Yangtze River Basin, and can be used to predict the future runoff sequences. The daily observed and simulated flow processes at the Yichang Station are shown in Fig. 9.

The future rainfall and temperature data are taken as inputs to the VIC hydrological model, and the future daily runoff data of each station were predicted by the proposed model. Then the changes of predicted runoff under different RCPs scenarios at each station were analyzed. The predicted runoff at the Yichang station under different RCPs scenarios are shown in Fig. 10 and Table 9.

As shown in Table 9, all the predicted runoff values lightly reduce in 2020 s, compared with the baseline runoff data. For the periods of 2050 s and 2080 s, the change rates of runoff are bigger than 0 except under RCP2.6 scenario. Under RCP2.6 scenario, it shows that the trend of runoff increases first and then decreases. Under RCP4.5 and RCP 8.5 scenarios, the trends of runoff are similar, both increase all the time. However, the change rate of runoff is smaller under RCP4.5 scenario, whose maximum change rate is 1.8%, while the maximum change rate is 14.0% under RCP8.5 scenario, both occurred in 2080 s. The trends of runoff under different RCPs scenarios are similar to that of rainfall and temperatures.

4.3. Prediction of future hydropower generation capacity of reservoir system

The optimal operation model of large-scale reservoirs in the upper Yangtze River Basin which includes 62 reservoirs was established. And the future runoff data simulated by the VIC hydrological model were used as inputs of the optimal operation model to calculate the future hydropower generation of the reservoir system. Fig. 11 shows the annual hydropower generation under different RCPs scenarios. And the average annual hydropower generation of reservoirs in the upper Yangtze River Basin under different RCPs scenarios are shown in Table 10.

It can be seen from Fig. 11 that there is a good positive correlation between the trend of hydropower generation and runoff. Under RCP2.6 and RCP4.5 scenarios, the slopes of fitting line of annual hydropower generation are small, while the slope of RCP8.5 scenario is obviously large.

As shown in Table 10, the predicted average annual hydropower generation of reservoirs from 2018 to 2100 under RCP2.6, RCP4.5 and RCP8.5 scenarios are 699.8 billion kW•h, 715.3 billion kW•h and 747.7 billion kW•h, respectively. For RCP2.6 scenario, the hydropower generation of the reservoir system will increase by 3.7% from 2020 s to 2050 s, and decrease by 1.66% from 2050 s to 2080 s, which is relatively stable. This trend of hydropower generation is the same as that of runoff evolution processes due to the close relationship between the hydropower generation and runoff. Under RCP4.5 scenario, the hydropower generation of 2050 s and 2080 s increases by 2.1% and 2.3% respectively, which shows a slowly increasing trend compared with their previous periods. While under RCP8.5 scenario, the hydropower generation of the basin shows a rapid growth trend, increasing 3.4% in 2050 s compared to 2020 s, and 11.7% in 2080 s compared to 2050 s. Results of the hydropower generation are consistent with the results of runoff simulation. The higher the RCP scenario is, the faster the runoff and hydropower generation increases. The average future hydropower generation of each reservoir under different RCP scenarios are shown in Fig. 12.

5. Conclusions and discussions

In this paper, the GCMs data was processed by SDSM downscaling method, and the future climate evolution trends of weather variables under different RCPs emission scenarios were predicted. Then, the macro-scale VIC hydrological model of the upper Yangtze River Basin was established, and the response of the runoff to climate change in the

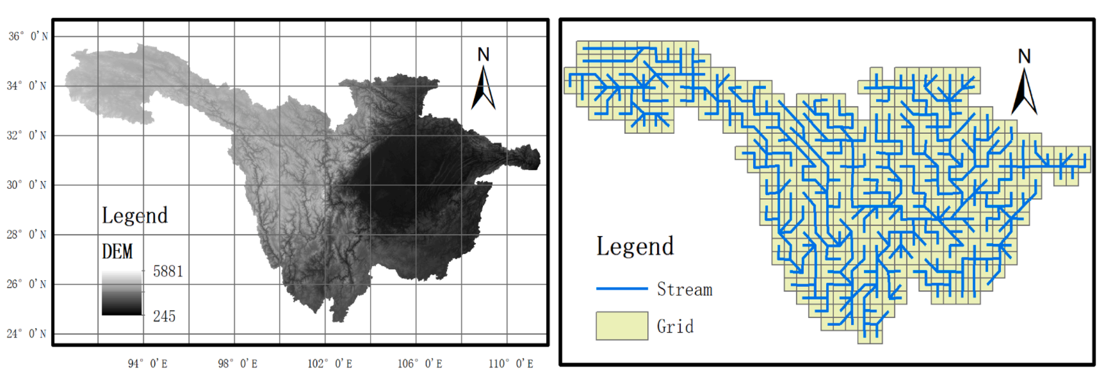

(a) The DEM data **(b)** Stream directions of each grid

Fig. 6. The DEM data and stream directions of each grid of study area.

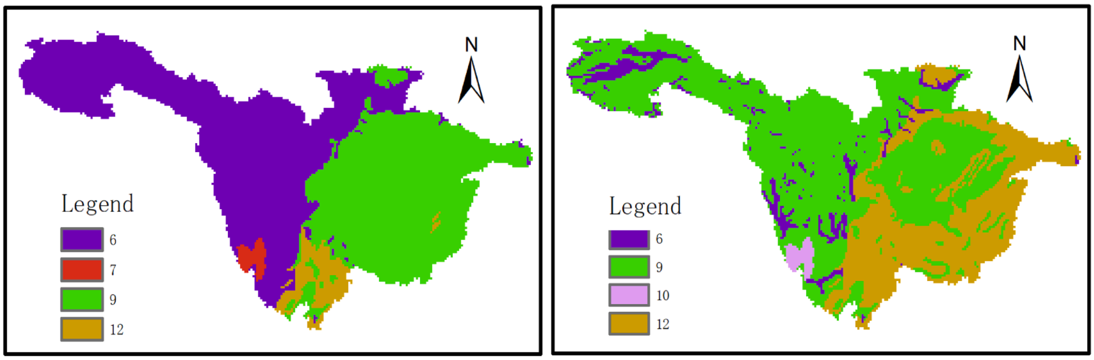

(a) Distribution of the upper soil **(b)** Distribution of the lower soil

Fig. 7. The upper soil and lower soil data of the study area.

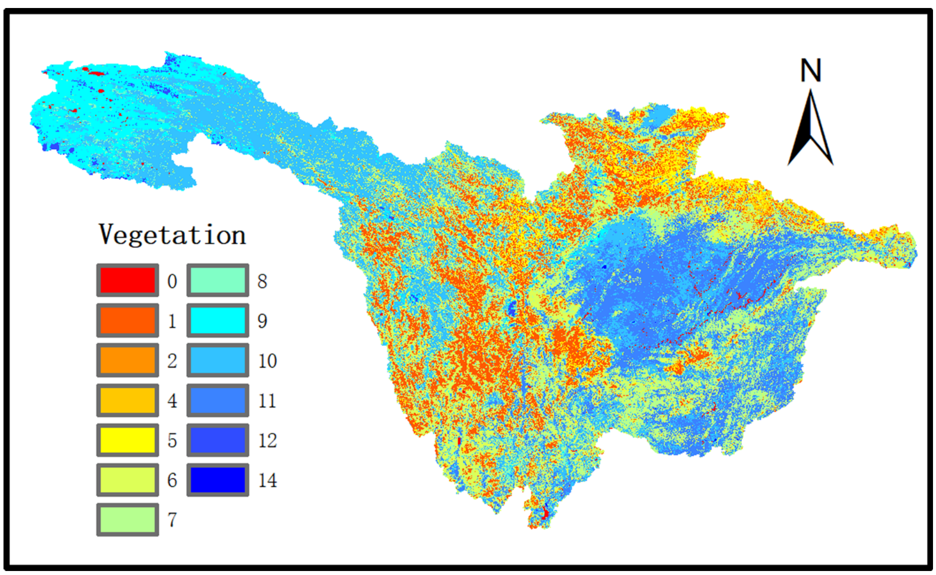

Fig. 8. The vegetation data of the study area.

Table 5
Proportions of different soil types of upper and lower soil.

Number	Types	Upper soil	Lower soil
6	Loam	54.32%	7.98%
7	Sandy clay loam	1.33%	0.00%
9	Clay loam	39.47%	60.09%
10	Sandy clay	0.00%	1.33%
12	Clay	4.88%	30.60%

upper Yangtze River Basin were investigated. The future runoff data were taken as input, the maximum annual hydropower generation were taken as the objective function. The optimal operation model of large-scale reservoirs including 62 reservoirs in the upper Yangtze River Basin was established, and the evolution trends of future hydropower generation under climate change were discussed. The main results are summarized as follows.

(1) The General Circulation Models and statistical downscaling model can be used to predict the future meteorological data. The predicted weather data can provide a reference for the study on temporal and spatial distribution of water resources in the upper Yangtze River Basin under climate change.

(2) The VIC hydrological model also shows a good performance for daily and monthly runoff simulations for the upper Yangtze River Basin. Simulation results demonstrate the evolution trends and the uncertainties of future runoff under different scenarios. Especially, the inflow situation and extreme hydrological phenomena, such as floods and droughts, are important input data for reservoir operation. Thus, the runoff series predicted in this paper can provide data support for flood control, water supply and hydropower generation operation of

Table 6
Proportions of different vegetation types in the study area.

Number	1	2	4	5	6	7
Types	Evergreen coniferous forest	Evergreen broad-leaf forest	Deciduous broad-leaf forest	Mixed forest	Woodland	Woody savannas
proportion (%)	11.98	0.08	1.48	3.28	14.57	16.68
Number	8	9	10	11	0,12,14	
Types	Thicket	Shrubbery	Grassland	Cropland	Water bodies, barren, urban	
proportion (%)	0.61	7.51	27.08	14.05	2.68	

Table 7
Parameter sensitivity analysis of each station.

Parameters	S_{sen} values of each Station Shigu	Panzhihua	Xiluodu	Xiangjiaba	Zhutuo	Cuntan	Yichang	Average
b	0.236	0.140	0.144	0.121	0.139	0.147	0.168	0.157
D_s	0.118	0.220	0.110	0.028	0.109	0.095	0.167	0.121
D_m	0.072	0.070	0.099	0.041	0.111	0.094	0.153	0.091
W_s	0.071	0.117	0.194	0.077	0.159	0.128	0.105	0.121
d_1	0.158	0.091	0.066	0.029	0.085	0.079	0.360	0.124
d_2	1.750	1.919	0.783	1.726	0.939	1.077	1.215	1.344
d_3	0.057	0.082	0.178	0.066	0.135	0.108	0.102	0.104

Table 8
Nash efficiency coefficients and flow relative errors of each station.

stations		Shigu	Panzhihua	Xiluodu	Xiangjiaba	Zhutuo	Cuntan	Yichang
Calibration period	NSE	0.832	0.812	0.857	0.851	0.878	0.871	0.720
	NSE_{mon}	0.905	0.946	0.950	0.950	0.948	0.945	0.936
	e_{all}	0.146	0.042	0.037	0.010	0.021	0.020	0.004
Validation period	NSE	0.833	0.835	0.876	0.872	0.883	0.865	0.759
	NSE_{mon}	0.875	0.962	0.987	0.981	0.979	0.976	0.947
	e_{all}	0.061	0.025	0.040	0.056	0.065	0.056	0.037

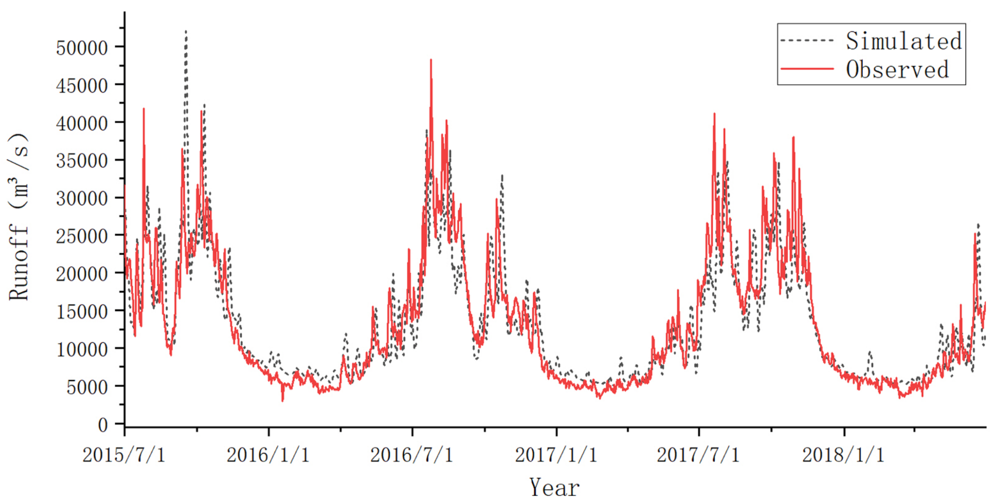

Fig. 9. The daily observed and simulated flow at Yichang station.

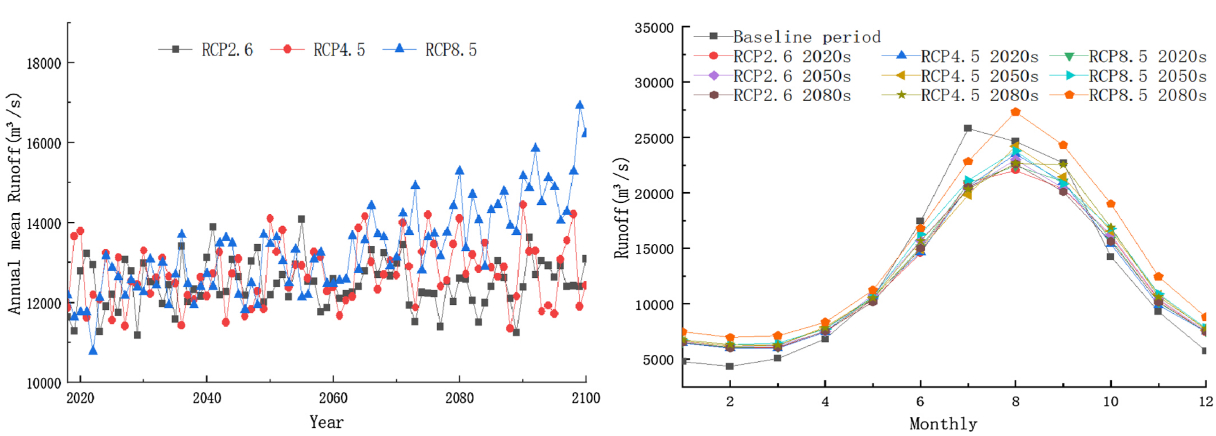

Fig. 10. The predicted runoff results under different RCPs scenarios at Yichang station.

reservoirs under different scenarios.

(3) In this study, the changes of the hydropower generation in the upper Yangtze River Basin in the future are small under RCP2.6 and RCP4.5 scenarios. While under RCP8.5 scenario, there is a significant increasing trend. It means that hydropower generation in the upper Yangtze River Basin is sensitive to climate change. Located in the west of China, the upper Yangtze River Basin is a region with abundant water resources, the increase of hydropower generation can promote the

Table 9
Predicted runoff results at the Yichang station under different RCP scenarios.

Stations	Periods	Baseline mean value (m^3/s)	Predicted mean value (m^3/s)			Change rate (%)		
			RCP2.6	RCP4.5	RCP8.5	RCP2.6	RCP4.5	RCP8.5
Yichang	2020 s	12,625	12,346	12,423	12,467	−2.2%	−1.6%	−1.3%
	2050 s	12,625	12,594	12,752	12,957	−0.2%	1.0%	2.6%
	2080 s	12,625	12,331	12,857	14,398	−2.3%	1.8%	14.0%

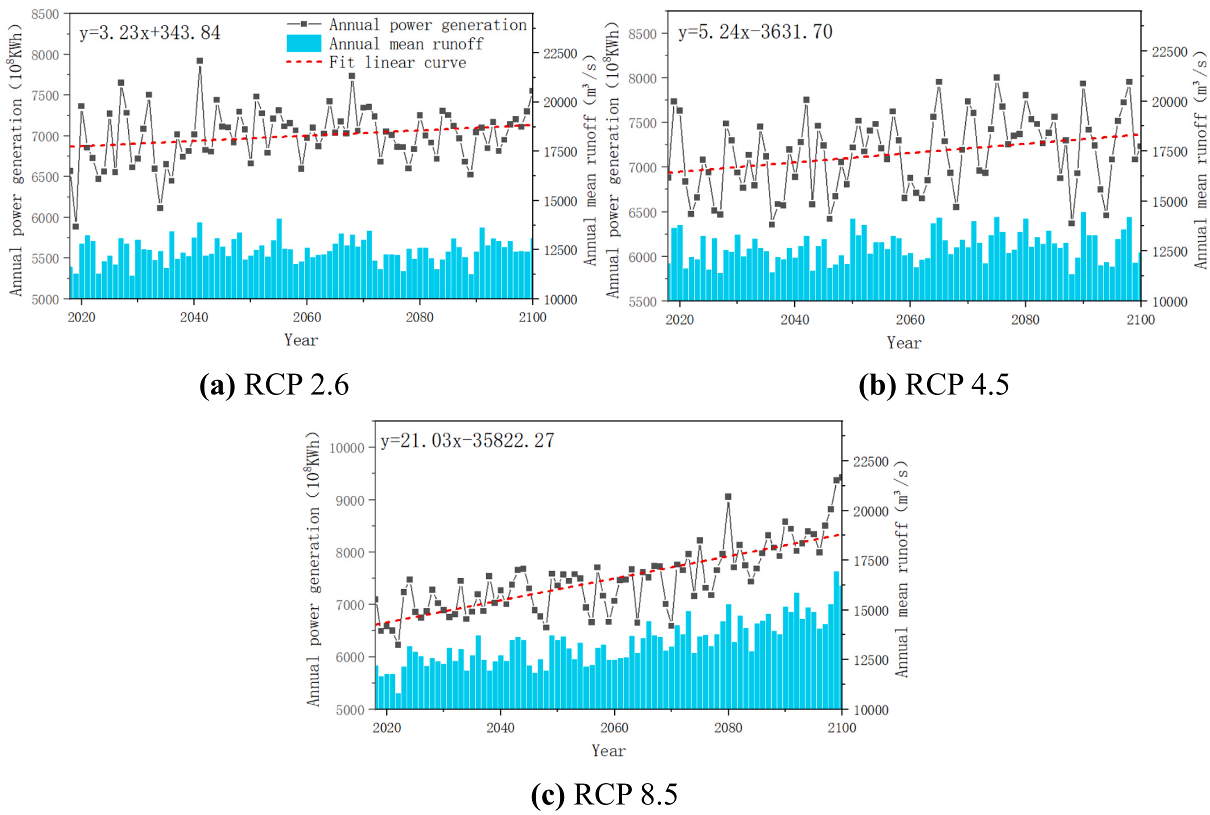

Fig. 11. Future annual hydropower generation under different RCPs scenarios.

Table 10
Average annual hydropower generation of reservoirs in the upper Yangtze River Basin.

Periods	Average annual hydropower generation(10^8 kW•h)		
	RCP2.6	RCP4.5	RCP8.5
2020 s	6870	6998	7017
2050 s	7122	7142	7257
2080 s	7004	7307	8109
All periods	6998	7153	7477

socioeconomic development of the region, and the power can also be delivered to the surrounding and eastern regions where the energy is relatively scarce. Meanwhile, the increase of hydropower means that the proportion of hydropower in the power system may increase, the proportion of fossil energy such as coal may be reduced, which not only protects the environment, but also slows down the consumption of non-renewable resources.

It is worth mentioning that at present, the calculation of hydropower generation is mainly based on the built and under construction reservoirs in the upper Yangtze River Basin. With the further development of hydropower, the hydropower generation in the upper Yangtze River has a trend of continuous growth, but the impact of climate change on hydropower generation is consistent. And the current hydropower development in the upper Yangtze River is close to the upper limit. Thus, this paper can provide a reference for the hydropower generation prediction under climate change in the upper Yangtze River.

The transferability of models used in this study to other regions was discussed. The SDSM model is easy to build and has good transferability (Sun et al., 2013). As for the VIC model, the transferability of hydrological models to other regions has always been a hot topic. Generally, the underlying surface and hydrometeorology conditions of regions are quite different, which lead to the difference of model parameters, and makes it difficult to transfer hydrological models to other regions. There are recommendations if someone want to embark on a future study using these models in a region similar to the case study. For the SDSM model, due to its good transferability, it is important to pay attention to obtaining the historical meteorological data of the region as much as possible, and ensure the reliability of the data to improve the effect of model calibration. For the VIC model, there are the following suggestions. If the hydrometeorology situation and underlying surface conditions of the target area are similar to those of the studied basin, the VIC model can be considered, and the model parameters calibrated in the studied basin can be taken as the initial value for further calibration. If their spatial location is close, the target basin is a sub-basin of the studied basin, the model parameters can be obtained by averaging the calibrated parameters of immediate upstream and

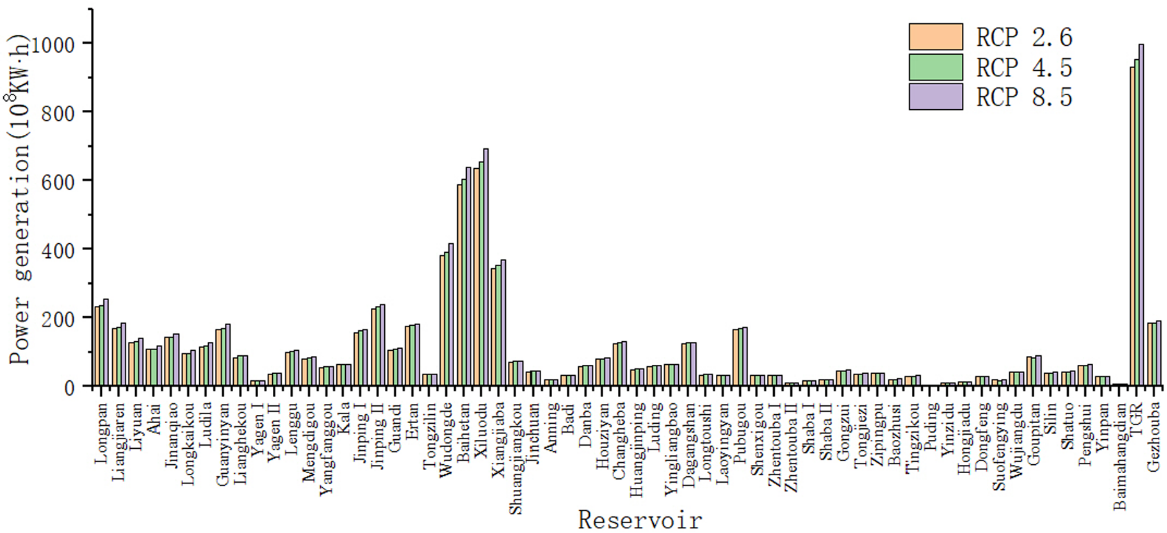

Fig. 12. The mean future hydropower generation of each reservoir under different RCPs scenarios.

downstream sub-basins of the studied basin, or by interpolating the parameters values of several other sub-basins with interpolation methods, such as kriging (Merz and Blöschl, 2004). In addition, the spatial resolution of DEM data and the density of basin grids affect the precision of the model. High-resolution DEM data and appropriate grid density can improve the precision of model and avoid excessive calculation. For the operation model of large-scale reservoirs, scholars need to fully grasp the distribution of reservoirs and their characteristic information in the target basin, which is the key factor for building the model.

There are still some limitations in this study, which need to be improved in the further study. When using SDSM model to downscale the GCMs, multiple GCMs can be considered to improve the reliability of the prediction of future climate change, and avoid the accidental errors caused by single model. These errors are mainly because the applicability of the model in the study area is unknown. This may lead to the deviation of prediction results, such as the poor correlation between the predicted temperature data and the observed data. The using of multiple GCMs can avoid the potential accidental error of a single model, but the regional applicability of various GCMs is different. Improper GCMs combination may affect the prediction results, and the calculation of multiple GCMs data is much larger, using multiple GCMs for climate prediction is more difficult than a single model. At the same time, past studies have shown that a single model suitable for the study area can also achieve good results. After summarizing the previous researches, we found that the CanESM2 model has been widely used in China's climate prediction, and has better applicability than most other models (Su et al., 2013; Chen et al., 2011; Chen and Frauenfeld, 2014). Using only the CanESM2 model was also adopted by many scholars (Wen et al., 2013; Lin et al., 2018; Tahir et al., 2018). Therefore, the CanESM2 model was selected to predict the future climate change in this paper. Results proved that its performance in this paper is also good. In addition, adding more applicable GCMs model may further improve the reliability and stability of prediction. Besides, due to the limitation of hydrometeorology data, the data length used for calibration of VIC model is relatively short, and increasing the data length can help optimize the calibration results of the model. In addition, the changes in underlying surface conditions over time, such as land use, were not considered in the calibration of VIC model. In the future study, the changes in underlying surface conditions can be considered properly to better simulate the true conditions of the basin.

CRediT authorship contribution statement

Wenjie Zhong: Software, Validation, Writing - original draft, Visualization. **Jing Guo:** Investigation, Formal analysis. **Lu Chen:** Conceptualization, Methodology, Project administration, Funding acquisition, Writing - original draft. **Jianzhong Zhou:** Resources, Supervision. **Junhong Zhang:** Data curation, Writing - review & editing. **Dangwei Wang:** Resources.

Declaration of Competing Interest

The authors declare that they have no known competing financial interests or personal relationships that could have appeared to influence the work reported in this paper.

Acknowledgments

The work in this paper was supported by the National Nature Science Foundation of China (51922047, 51879109, 5169094 and 91547208) and the State Key Laboratory of Simulation and Regulation of Water Cycle in River Basin of China (SKL2020ZY08), the Fundamental Research Funds for the Central Universities (2017KFYXJJ194, 2019kfyRCPY057).

References

Afshar, M.H., 2013. Extension of the constrained particle swarm optimization algorithm to optimal operation of multi-reservoirs system. Int. J. Electr. Power Energy Syst. 51, 71–81.

Birkinshaw, S.J., Guerreiro, S.B., Nicholson, A., Liang, Q., Quinn, P., Zhang, L., He, B., Yin, J., Fowler, H.J., 2017. Climate change impacts on Yangtze River discharge at the Three Gorges Dam. Hydrology and Earth System Science 1911–1927.

Chang, X., Liu, X., Zhou, W., 2010. Hydropower in China at present and its further development. Energy 35 (11), 4400–4406.

Charles, S.P., Bates, B.C., Hughes, J.P., 1999. A spatiotemporal model for downscaling precipitation occurrence and amounts. Journal of Geophysical Research-Atmospheres 104 (D24), 31657–31669.

Chen, H., Xiang, T., Zhou, X., Xu, C.Y., 2012. Impacts of climate change on the Qingjiang Watershed's runoff change trend in China. Stoch. Env. Res. Risk Assess. 26 (6), 847–858.

Chen, J., Li, Q., Niu, J., Sun, L., 2010. Regional climate change and local urbanization effects on weather variables in Southeast China. Stoch. Env. Res. Risk Assess. 25 (4), 555–565.

Chen, J., Niu, J., Sun, L., 2013. Water Resources of Mainland China. Climate Vulnerability 195–211.

Chen, J., Shi, H., Sivakumar, B., Peart, M.R., 2016. Population, water, food, energy and dams. Renew. Sustain. Energy Rev. 56, 18–28.

Chen, L., Sun, N., Zhou, C., Zhou, J., Zhou, Y., Zhou, J., Zhou, Q., 2018. Flood Forecasting Based on an Improved Extreme Learning Machine Model Combined with the

Backtracking Search Optimization Algorithm. Water 10 (10), 1362.
Chen, L., Ye, L., Singh, V.P., Zhou, J., Guo, S., 2014a. Determination of Input for Artificial Neural Networks for Flood Forecasting Using the Copula Entropy Method. J. Hydrol. Eng. 19 (11).
Chen, L., Singh, V.P., Guo, S., Zhou, J., Ye, L., 2014b. Copula entropy coupled with artificial neural network for rainfall-runoff simulation. Stoch. Env. Res. Risk Assess. 28 (7), 1755–1767.
Chen, L., Frauenfeld, O.W., 2014. Surface Air Temperature Changes over the Twentieth and Twenty-First Centuries in China Simulated by 20 CMIP5 Models. J. Clim. 27 (11), 3920–3937.
Chen, L., Huang, K., Zhou, J., Duan, H., Zhang, J., Wang, D., Qiu, H., 2020. Multiple-risk assessment of water supply, hydropower and environment nexus in the water resources system. J. Cleaner Prod In press.
Chen, W., Jiang, Z., Li, L., 2011. Probabilistic Projections of Climate Change over China under the SRES A1B Scenario Using 28 AOGCMs. J. Clim. 24 (17), 4741–4756.
Cheng, C.T., Wang, S., Chau, K.W., Wu, X.Y., 2014. Parallel discrete differential dynamic programming for multireservoir operation. Environ. Modell. Software 57, 152–164.
Choi, J. Y., Choi, C. H. 1992. Sensitivity analysis of multilayer perceptron with differentiable activation functions. IEEE Transactions on Neural Networks, 1992, 3(1), 101-107.
Chu, H.B., Wei, J.H., Li, T.J., Jia, K., 2016. Application of support vector regression for mid- and long-term runoff forecasting in “Yellow River Headwater” Region. Procedia Eng. 154, 1251–1257.
Cohen, G., 1978. Optimization by decomposition and coordination: a unified approach. IEEE Trans. Autom. Control 23 (2), 222–232.
Fan, J., Hu, J., Zhang, X., Kong, L., Li, F., Mi, Z., 2018. Impacts of climate change on hydropower generation in China. Math. Comput. Simul 167, 4–18.
Feng, Z.K., Niu, W.J., Cheng, C.T., 2017. A Quadratic Programming Approach for Fixed Head Hydropower System Operation Optimization Considering Power Shortage Aspect. J. Water Resour. Plann. Manage. 143 (10).
Hassan, Z., Shamsudin, S., Harun, S., 2014. Application of SDSM and LARS-WG for simulating and downscaling of rainfall and temperature. Theor. Appl. Climatol. 116 (1–2), 243–257.
Howson, H.R., Sancho, N.G.F., 1975. A new algorithm for the solution of multi-state dynamic programming problems. Math. Program. 8, 114–116.
Huntington, T.G., 2006. Evidence for intensification of the global water cycle: Review and synthesis. J. Hydrol. 319 (1–4), 83–95.
Kao, S.C., Sale, M.J., Ashfaq, M., Martinez, R.U., Kaiser, D.P., Wei, Y., Diffenbaugh, N.S., 2015. Projecting changes in annual hydropower generation using regional runoff data: An assessment of the United States federal hydropower plants. Energy 80, 239–250.
Klausmeyer, K.R., Shaw, M.R., 2009. Climate Change, Habitat Loss, Protected Areas and the Climate Adaptation Potential of Species in Mediterranean Ecosystems Worldwide. PLoS ONE 4 (7), e6392.
Li, G., Sun, Y.J., He, Y., Li, X.F., Tu, Q.Y., 2014a. Short-Term Power Generation Energy Forecasting Model for Small Hydropower Stations Using GA-SVM. Mathematical Problems in Engineering 1–9.
Li, C.L., Zhou, J.Z., Ouyang, S., Ding, X.L., Chen, L., 2014b. Improved decomposition–coordination and discrete differential dynamic programming for optimization of large-scale hydropower system. Energy Convers. Manage. 84, 363–373.
Li, X., Chen, Z., Fan, X., Cheng, Z., 2018. Hydropower development situation and prospects in China. Renew. Sustain. Energy Rev. 82, 232–239.
Lin, P., He, Z.B., Du, J., Chen, L., Zhu, X., Li, J., 2018. Impacts of climate change on reference evapotranspiration in the Qilian Mountains of China: Historical trends and projected changes. Int. J. Climatol. 38 (7), 2980–2993.
Liu, W.F., Xu, Z.X., Li, F.P., Zhang, L.Y., Zhao, J., Yang, H., 2015a. Impacts of climate change on hydrological processes in the Tibetan Plateau: a case study in the Lhasa River basin. Stoch. Env. Res. Risk Assess. 29 (7), 1809–1822.
Liu, P., Li, L.P., Guo, S.L., Xiong, L.H., Zhang, W., Zhang, J.H., Xu, C.Y., 2015b. Optimal design of seasonal flood limited water levels and its application for the Three Gorges Reservoir. J. Hydrol. 527, 1045–1053.
Liu, X., Tang, Q., Voisin, N., Cui, H., 2016. Projected impacts of climate change on hydropower potential in China. Hydrol. Earth Syst. Sci. 20 (8), 3343–3359.
Madani, K., Guégan, M., Uvo, C.B., 2014. Climate change impacts on high-elevation hydroelectricity in California. J. Hydrol. 510, 153–163.
Merz, R., Blöschl, G., 2004. Regionalisation of catchment model parameters. J. Hydrol. 287 (1–4), 95–123.
Moreno, J., 2009. Hydraulic plant generation forecasting in Colombian power market using ANFIS. Energy Econ. 31, 450–455.
Nijssen, B., O'Donnell, G.M., Lettenmaier, D.P., Wood, E.F., 2001. Predicting the discharge of global rivers. J. Clim. 14, 3307–3323.
Nilawar, A.P., Waikar, M.L., 2019. Impacts of climate change on streamflow and sediment concentration under RCP4.5 and 8.5: a case study in Purna river basin. India. Science of The Total Environment 650, 2685–2696.
Nourani, V., Hosseini Baghanam, A., Adamowski, J., Kisi, O., 2014. Applications of hybrid wavelet–Artificial Intelligence models in hydrology: A review. J. Hydrol. 514, 358–377.
Qin, P., Xu, H., Liu, M., Du, L., Xiao, C., Liu, L., Tarroja, B., 2020. Climate change impacts on Three Gorges Reservoir impoundment and hydropower generation. J. Hydrol. 580, 123922.
Raje, D., Mujumdar, P.P., 2010. Reservoir performance under uncertainty in hydrologic impacts of climate change. Adv. Water Resour. 33 (3), 312–326. https://doi.org/10.1016/j.advwatres.2009.12.008.
Shi, H., Chen, J., Liu, S., Sivakumar, B., 2019. The Role of Large Dams in Promoting Economic Development under the Pressure of Population Growth. Sustainability 11 (10), 2965.
Shi, H., Wang, G., 2015. Impacts of climate change and hydraulic structures on runoff and sediment discharge in the middle Yellow River. Hydrol. Process. 29 (14), 3236–3246.
Solomatine, D.P., Maskey, M., Shrestha, D.L., 2007. Instance-based learning compared to other data-driven methods in hydrological forecasting. Hydrol. Process. 22 (2), 275–287.
Srikanthan, R., McMahon, T.A., 2001. Stochastic generation of annual, monthly and daily climate data: a review. Hydrology and Earth Systems Sciences 5 (4), 653–670. https://doi.org/10.5194/hess-5-653-2001.
Su, F., Adam, J.C., Bowling, L.C., Lettenmaier, D.P., 2005. Streamflow simulations of the terrestrial arctic domain. Journal of Geophysical Research: Atmospheres 110 (D8), D08112.
Su, F., Duan, X., Chen, D., Hao, Z., Cuo, L., 2013. Evaluation of the global climate models in the cmip5 over the tibetan plateau. J. Clim. 26 (10), 3187–3208.
Sun, J., Lei, X., Tian, Y., Liao, W., Wang, Y., 2013. Hydrological impacts of climate change in the upper reaches of the Yangtze River Basin. Quat. Int. 304, 62–74.
Tahir, T., Hashim, A.M., Yusof, K.W., 2018. Statistical downscaling of rainfall under transitional climate in Limbang River Basin by using SDSM. Iop Conference 140, 012037.
Tao, X., Chen, H., Xu, C., Hou, Y., Jie, M., 2015. Analysis and prediction of reference evapotranspiration with climate change in Xiangjiang River Basin. China. Water Science and Engineering 8 (4), 273–281.
van Vliet, M.T.H., Wiberg, D., Leduc, S., Riahi, K., 2016. Power-generation system vulnerability and adaptation to changes in climate and water resources. Nat. Clim. Change 6 (4), 375–380.
Wen, H.Q., Zhang, X., Xu, Y., Wang, B., 2013. Detecting human influence on extreme temperatures in China. Geophys. Res. Lett. 40 (6), 1171–1176.
Wilby, R.L., Hassan, H., Hanaki, K., 1998. Statistical downscaling of hydrometeorological variables using general circulation model output. J. Hydrol. 205 (1–2), 1–19.
Wilby, R.L., Hay, L.E., Leavesley, G.H., 1999. A comparison of downscaled and raw GCM output: implications for climate change scenarios in the San Juan River basin. Colorado. Journal of Hydrology 225 (1–2), 67–91.
Wood, A.W., Leung, L.R., Sridhar, V., Lettenmaier, D.P., 2004. Hydrologic Implications of Dynamical and Statistical Approaches to Downscaling Climate Model Outputs. Clim. Change 62 (1–3), 189–216.
Yang, G., Guo, S., Li, L., Hong, X., Wang, L., 2015. Multi-Objective Operating Rules for Danjiangkou Reservoir Under Climate Change. Water Resour. Manage. 30 (3), 1183–1202.
Zhang, Y.Q., You, Q.L., Chen, C.C., Ge, J., 2016. Impacts of climate change on streamflows under RCP scenarios: A case study in Xin River Basin, China. Atmos. Res. 178–179, 521–534.
Zhou, C., Sun, N., Chen, L., Ding, Y., Zhou, J.Z., Zha, G., Luo, G.L., Dai, L., Yang, X., 2018. Optimal operation of cascade reservoirs for flood control of multiple areas downstream: A case study in the upper Yangtze river basin. Water 10 (9), 1250.
Zhou, Y., Hejazi, M., Smith, S., Edmonds, J., Li, H., Clarke, L., Calvin, K., Thomson, A., 2015. A comprehensive view of global potential for hydro-generated electricity. Energy Environ. Sci. 8 (9), 2622–2633.
Zorita, E., von Storch, H., 1999. The Analog Method as a Simple Statistical Downscaling Technique: Comparison with More Complicated Methods. J. Clim. 12 (8), 2474–2489.